Title

Dust storm-driven dispersal of potential pathogens and antimicrobial resistance genes in the Eastern Mediterranean

Authors

Burak A. Erkorkmaz,[1] David Zeevi,[2] and Yinon Rudich[1]*

Affiliations

[1]Department of Earth and Planetary Sciences, Weizmann Institute of Science, Rehovot 7610001, Israel

[2]Department of Plant and Environmental Sciences, Weizmann Institute of Science, Rehovot 7610001, Israel

*Yinon Rudich

Email: yinon.rudich@weizmann.ac.il

Abstract

The atmosphere hosts a microbiome that connects remote ecosystems but remains underexplored. In this study, we employed metagenomics to examine the ecological roles of the atmospheric microbiome, including the dispersal of potential pathogens and antibiotic resistance genes, and its response to temperature fluctuations and dust storms intensified by climate change. We analyzed air samples from non-dusty conditions and Middle Eastern dust storms, identifying several facultative pathogens like *Klebsiella pneumoniae*, *Stenotrophomonas maltophilia*, and *Aspergillus fumigatus*, linked to human respiratory diseases, and others like *Zymoseptoria tritici*, *Fusarium poae*, and *Puccinia striiformis*, harmful to wheat, associated with dust storms and rising temperatures. We observed increased functions related to antibiotic resistance, including beta-lactams, aminoglycosides, and fluoroquinolones, and virulence factors during dust storms. Our findings suggest that dust storms may spread these traits. Continuous monitoring is crucial to understand the broader implications of dust storms and temperature increases on the atmospheric microbiome amid climate change, emphasizing the need for a One Health approach to global climate challenges.

Teaser

Atmospheric microbiome analysis reveals climate change-fueled dust storms spread human, animal, and plant pathogens.

MAIN TEXT

Introduction

The atmosphere harbors a microbiome that holds significant importance for Earth's ecosystems (*1*). Despite its fundamental role, the atmospheric microbiome remains one of the least explored ecosystems concerning its microbial traits and the factors influencing its dynamics, as well as its potential impacts on ecology and health. The atmospheric microbiome is remarkably diverse and dynamic, comprising microorganisms from various sources. Some are naturally emitted through mechanisms like wind and oceanic aerosolization, while others originate from anthropogenic activities such as industrial processes, agriculture, and transportation (*2-4*). Notably, dust storms act as carriers, lifting substantial amounts of particles from arid regions and transporting microorganisms over great distances (*5, 6*). This process significantly alters the ecological composition and dynamics of the atmospheric microbiome by introducing new microbial entities into this system and facilitating connections between geographically distant areas (*7-9*). Dust carries a wide array of soil microorganisms, leading to a significant increase in microbial abundance in the atmosphere under dusty conditions (*7, 8, 10*). Upon settling, dust can impact both terrestrial and aquatic ecosystems (*11, 12*). The presence of potentially harmful microorganisms in transported dust might pose diverse risks to public and ecosystem health (*7, 8, 13*). Previous research has documented the dispersal of pathogens over long distances in the atmosphere, thereby contributing to various plant diseases (*14-16*). Additionally, numerous epidemiologic studies have linked dust storms to human diseases, particularly respiratory issues (*17-23*). This raises concerns about the potential biological causative agents in dust triggering these diseases. Furthermore, while the spread of antibiotic resistance is primarily associated with hospitals due to extended medication use, genes linked to antibiotic resistance are found in various environments, including in airborne dust (*7, 8*). This finding suggests the atmosphere as a potential conduit for gene dispersion across distant locales. Therefore, it is crucial to determine the extent to which dust storms carry potential pathogenic agents and whether they host factors associated with antibiotic resistance and pathogenicity. This is especially important as climate change is projected to increase particulate matter concentrations and lead to more frequent dust events, especially in the Eastern Mediterranean region (*24, 25*). Additionally, the expansion of Hadley cells towards the poles is anticipated to exacerbate drying conditions and extend dust storms northward towards Europe (*24*). Therefore, understanding these dynamics is essential for assessing the potential impact of climate change on the atmospheric microbiome at both local and global scales.

Studying the atmospheric microbiome presents unique challenges due to its low-biomass nature (*26*). Overcoming this challenge requires sophisticated bioinformatic algorithms and high sequencing depth for accurate analysis. While traditional methods like amplicon sequencing, which target specific genetic markers such as the 16S ribosomal RNA gene and internal transcribed spacer (ITS), have been utilized to identify taxonomic features, they primarily limited to the genus level for bacteria and fungi (*7, 8, 10, 27*). Recent studies have employed shotgun metagenomic and metatranscriptomic sequencing in other ecologies to explore the atmospheric microbiome, utilizing advanced aerosol sampling devices and genomic technologies (*26, 28, 29*). However, most investigations of the dust microbiome have focused on shallow taxonomic characterization or have taken a generalized approach to functional characterization (*7, 8, 10, 27, 30, 31*), rather than tailoring bioinformatic tools that are specific to each scientific research question. Moreover, some studies have quantified fragments of a few known antibiotic resistance genes by qPCR, overlooking the broader

diversity, richness, and origin of these features within the atmospheric microbiome (*7, 8*). Furthermore, the sampling strategies employed in these studies lack longitudinal designs, which are crucial for capturing the dynamic nature of atmospheric conditions and their relationship with microbial features over time. Consequently, there is a clear need for comprehensive research on microbial traits in the atmosphere, especially under dusty conditions.

In this study, our primary objective is to understand how the composition of the air microbiome change over time in relation to shifting atmospheric conditions, particularly concerning its potential impacts on ecology and health. We focus on dust storms transporting microorganisms, including harmful pathogens, and investigate whether these pathogens carry genes associated with antibiotic resistance and virulence, which could pose risks to public health and the environment. Using metagenomic approaches, we assess the influence of key environmental factors, such as particulate matter concentration and temperature, which are intensifying due to climate change.

Results

Meteorological conditions before and during the sampling period and, the estimated origin of dust

We collected air samples from March 29th to May 31st, 2022, at the onset of the dry season after winter rainfalls. We did not record any precipitation during this period (Fig. S1). Temperatures steadily increased during the campaign, ranging from 16.5 to 27.1°C (Fig. S2). We defined dust events using a daily mean PM_{10} concentration threshold of 65.2 µg m^{-3}, based on a recent study conducted in the EM (*32*). Over the sampling period, only fifteen days exceeded this threshold, indicating dusty conditions. We identified three distinct air transport patterns using dust column mass density maps and back trajectory analysis of air masses: northwesterly, southwesterly, and easterly (Movies S1-S4). Further details about this analysis are provided in the Supplementary Materials. In summary, we collected a total of forty-five air samples during the sampling period, comprising both dusty (n=13) and clear (n=32) atmospheric conditions (Fig. S2 and Dataset S1).

Abundance, richness, and diversity of the atmospheric microbiome

We observed variations in the total sampled biomass, as measured by the total DNA yield obtained from air samples, with significantly higher concentrations found in dusty atmospheric conditions (2.10±4.43 ng μL^{-1}, mean±SD) compared to clear atmospheric conditions (0.31±0.33 ng μL^{-1}) (Mann–Whitney *U* test, $p<0.001$, Fig. S3). Due to the inherently low biomass nature of air samples, we did not obtain sufficient DNA for both genomic sequencing analysis and qPCR analysis. qPCR provides a more sensitive measure of biomass compared to fluorometric analysis as in Qubit. This limitation is particularly relevant when studying dust storms, as the sampling window to capture the storm at its peak is typically limited to a few hours. However, this finding is consistent with previous qPCR quantifications from our earlier studies, which used longer sampling times that compromised the specificity of dust storms. These earlier studies also demonstrated an increased absolute abundance on dusty days, indicating a higher microbial abundance in dusty conditions compared to clear days (*7, 8, 10*).

We found that only a small portion of the total reads identified with a known taxonomy (3.81±3.37%, mean±SD, Fig. S4). Bacteria predominantly comprised the atmospheric microbial community, accounting for 95.8±1.94% (mean±SD) of the assigned reads, while fungi, archaea, other eukaryotes, and viruses constituted minor proportions across all

samples (3.79±1.8%, 0.12±0.31%, and 0.12±0.22%, respectively, Fig. S5). Notably, specific bacterial classes, including Actinomycetes (49.0±10.4%, mean±SD), Gammaproteobacteria (17.9±10.3%), and Alphaproteobacteria (15.5±3.57%), emerged as dominant taxa within the atmospheric microbial community (Fig. S6).

We observed variations in the composition of prominent microbial classes under different atmospheric conditions, as illustrated in Fig. S7. Dusty conditions showed significant increases in certain classes such as Actinomycetes (Mann–Whitney *U* test, p=0.068) and Rubrobacteria (p=0.006), known for their resilience to environmental stressors (*33*). Notably, *Geodermatophilus obscurus*, a prominent Actinomycetes species, exhibited distinct dominance in dusty conditions compared to clear ones (Mann–Whitney *U* test, p<0.001), constituting 16.7±11.2% (mean±SD) of the microbial community in dusty conditions and 4.97±3.85% in clear conditions (Fig. S8). Conversely, certain Hydrobacteria group microorganisms, including Alphaproteobacteria (Mann–Whitney *U* test, p<0.001) and Betaproteobacteria (p=0.055), showed increased relative abundance in clear atmospheric conditions, suggesting a stronger marine influence (*33*).

A variance partitioning analysis (Adonis) highlighted the impact of different environmental factors on the variability observed in the atmospheric microbiome composition. Daily mean PM_{10} concentration accounted for the highest proportion of total variation (9.8% for taxonomy, 8.8% for functional attributes), followed by mean temperature and air mass origin (temperature: 9.3% and 4.6%; air mass: 9.3% for taxonomy, but not functional attributes, Table S1). Notably, relative humidity did not contribute significantly to the variation.

We conducted Principal Coordinates Analysis (PCoA) using Bray–Curtis dissimilarity to explore microbial patterns within atmospheric samples. Our analysis revealed distinct patterns. Firstly, clear atmospheric conditions exhibited separate clustering of the microbiome compared to dusty atmospheric conditions, regardless of air-mass origin. This suggests a common microbial composition among samples from clear days despite variations in other factors. The significance of this finding was supported by a considerable dissimilarity between these two distinct communities (Adonis, R^2=0.09, p<0.001). Under dusty conditions, the atmospheric microbiome of southwesterly air masses partially clustered with the microbiome of clear conditions, while easterly air masses distinctly separated from clear conditions and southwesterly air masses. Essentially, the atmospheric microbiome on clear days tended to cluster together, whereas the microbiome on dusty days appeared less cohesive and not necessarily unified. Second, a clear temperature-related trend emerged, especially under clear atmospheric conditions, as indicated by a significant correlation between the first principal component (PCo1) and temperature (Pearson's correlation, r=0.44, p=0.002) (Fig. 1A and Fig. S9A). We observed similar, yet less distinct trends, in PCoA based on Bray–Curtis dissimilarity of the functional profile (see Fig. 1D and Fig. S9B). Additionally, the functional characteristics of the atmospheric microbiome exhibited distinct patterns across various functional sub-categories. For instance, we noted significant differences in SEED functional sub-categories for cell envelope (Adonis, R^2=0.14, p<0.001) and metabolism (R^2=0.09, p<0.001), with particularly pronounced variations observed in the stress response, defense, and virulence (R^2=0.12, p<0.001) (Fig. S10).

We also assessed the dissimilarity of air samples based on their taxonomic and functional profiles. The dissimilarity between samples regarding functional profiles was significantly

lower than that observed in the taxonomic profiles within the atmospheric microbiome (Mann–Whitney *U* test, $p<0.001$, Fig. S11). This observation suggests that functional characteristics are more robust than taxonomic traits in the atmospheric microbiome.

Dusty days were typically associated with elevated daily mean temperatures, as illustrated in Fig. S12 (Mann–Whitney *U* test, $p=0.008$). Our analyses, including PCoA and variance partitioning, emphasized PM_{10} concentration as the primary factor influencing community composition. Notably, during a major dust storm event originating from Eastern sources on April 24-26, 2022, we identified unique microbial features within the atmospheric microbiome for the first time. This dust storm lasted over three days, with PM_{10} concentrations exceeding 900 μg m^{-3}. It is conceivable that the microbial features transported by this intense dust storm might have impacted local ecosystems, potentially leading to the observation of new taxa in subsequent clear days within the atmosphere. Additionally, temperature exerted a secondary, albeit lesser, influence, becoming more pronounced towards the end of the sampling campaign. Consequently, distinguishing the effects of PM_{10} from temperature presents a challenge. To address this challenge, we evaluated the impact of dust storms and temperature across all samples, encompassing both clear and dusty days. However, to mitigate potential biases resulting from these combined effects that may confound correlation analysis, we conducted a separate analysis focusing exclusively on dusty days to discern the specific influence of PM_{10} concentration during such conditions.

The richness of the atmospheric microbial community, as measured by the count of identifiable species and functional attributes, did not exhibit a statistically significant difference between dusty and clear atmospheric conditions (Mann–Whitney *U* test, $p=0.37$ and $p=0.32$, respectively, Fig. 1B and 1E). In dusty atmospheric conditions, we observed a trend in both taxonomic and functional features suggesting increased richness with higher PM_{10} concentrations. However, this trend did not reach statistical significance (Pearson's correlation, $r=0.51$, $p=0.077$ and $r=0.54$, $p=0.055$). Conversely, during clear atmospheric conditions, we did not observe a significant trend (Pearson's correlation, $r=0.28$, $p=0.123$ and $r=0.18$, $p=0.312$, respectively), likely due to the narrow range of PM_{10} concentrations on those days. Notably, a significant positive correlation between species richness and increasing temperatures was evident throughout the sampling period for both taxonomic and functional features (Pearson's correlation, $r=0.40$, $p=0.006$ and $r=0.38$, $p=0.010$, respectively). This correlation was more pronounced when analyzing only clear day samples (Pearson's correlation, $r=0.64$, $p<0.001$ and $r=0.59$, $p<0.001$, respectively).

The Shannon–Wiener Diversity index of both taxonomic and functional attributes significantly decreased in the atmospheric microbial community during dusty conditions compared to clear conditions (Mann–Whitney *U* test, $p=0.007$ and $p=0.005$, Fig. 1C and 1F). This indicates that microbial communities in dusty atmospheric conditions were dominated by specific species and functions, resulting in a less even distribution of these features compared to clear atmospheric conditions. Moreover, there was no significant correlation between increasing PM_{10} concentrations and increasing diversity under dusty conditions (Pearson's correlation, $r=0.12$, $p=0.683$ and $r=0.25$, $p=0.410$). This suggests that the dominance of specific species and functions in the microbiome of dusty conditions was not associated with the dust load uplifted but rather influenced by potential ecological origins (i.e., desert compared to marine and local influences). In contrast, the diversity index increased with rising temperatures throughout the sampling period for taxonomic and functional features (Pearson's correlation, $r=0.35$, $p=0.019$ and $r=0.26$ $p=0.089$,

respectively) and specifically on clear days (r=0.58, p<0.001 and r=0.32, p=0.069, respectively), although it did not reach statistical significance regarding functional attributes. This implies that increasing temperatures not only enhanced the observed number of species and functions but also led to a more uniform increase in their abundance.

In summary, environmental variables, particularly dust storms, and to a lesser extent, temperature fluctuations, significantly shape both taxonomic and functional aspects of the atmospheric microbiome, while air mass origin specifically influences taxonomic composition.

Potential pathogens in the atmospheric microbiome

Observing the discernible patterns within the atmospheric microbiome under clear and dusty conditions, with particular emphasis on the distinctions in functional attributes linked to stress response, defense mechanisms, virulence, and cell envelope characteristics, we next examine the presence of microbial species known for their pathogenic potential in the context of human, animal, and plant health under varying atmospheric conditions. To conduct this analysis, we first complied a comprehensive list of known pathogenic microorganisms from various publicly available datasets, as detailed in the Supplementary Materials. We then compared this list to Kraken2 taxonomic classification results, refining the analysis with Bracken for read abundance. Using all complete reference genomes/proteins from diverse taxonomic groups (archaea, bacteria, viruses, fungi, and protozoa) sourced from the NCBI RefSeq database, we employed Kraken2's exact k-mer matching to identify taxa. This method identifies taxonomy based on unique k-mers specific to each taxon at a defined taxonomic level, prioritizing those with the highest leaf-to-ancestor weight. This approach allowed us to identify DNA fragments (reads) that matched each reference genome through marker k-mer matching, while excluding genomic regions overlapping between closely related species.

Our analysis revealed DNA fragments matching a total of 117 species with known pathogenicity in human, animal, and plant hosts. Bacteria constituted the majority with 86 species, followed by fungi (25 species), other eukaryotes (4 species), and viruses (2 species). Particularly, bacterial species *Stenotrophomonas maltophilia* (3.15±0.27; mean±SD, N=45; prevalence), *Pasteurella multocida* (3.03±0.18, N=45) and *Klebsiella pneumonia* (2.89±0.30, N=45), along with fungal species *Botrytis cinerea* (2.56±0.48, N=45), exhibited notably higher mean read abundance ($\log_{10}$(CPM)) and prevalence across all samples compared to other species. The results are presented in Fig. 2A. The normalized read abundance, expressed in counts per million (CPM), of bacterial, fungal, eukaryotic, and viral species in each sample is provided in Dataset S2.

To further examine these taxonomic assignments, we conducted read mapping within each air sample to the reference genome of the 34 most prevalent potential pathogens individually (Fig. 2). Additionally, we included *G. obscurus* as a reference due to its consistently high abundance across the sampling period, particularly in dusty conditions. The primary objective of this additional analysis was to ascertain whether the genomes of the identified pathogens were genuinely present or if the identifications were likely false positives. To achieve this, we analyzed the genome coverage and distribution of reads, as higher genome coverage and a uniform read distribution across the entire reference genome are indicative of the presence of these species in the air samples. We observed varying genome coverage, representing the percentage of all base pairs of the genome covered by reads, and depth, indicating the number of unique reads mapped to a specific nucleotide, for these species.

For instance, across all samples, approximately 30.0±19.8% (mean±SD) of the reference genome of *G. obscurus*, the generally most abundant taxon, was covered by reads. In comparison, the coverage for the most prevalent potential pathogens, despite their low abundance, was as follows: *S. maltophilia* 3.95±2.15%, *K. pneumonia* 2.38±3.16%, *B. cinerea* 1.54±2.29%, and *P. multocida* 0.84±0.22%. Moreover, we noted that the reads are uniformly distributed across the reference genome, although with a low mean depth, as shown in Fig. 3A and 3B. Detailed information on genome coverage and depth for each species can be found in Datasets S3-S5. These findings are consistent with KrakenUniq results, suggesting that Kraken's classifications were the result of marker k-mers distributed throughout the entire reference genome (Supplementary Materials, Dataset S6 and Fig. S13). Overall, these results validate the accuracy of taxonomic classification and assure the presence of these species in air samples. While read mapping results further assure the presence of these species in air samples, we recognize the limitations of using shotgun metagenomic data for identifying potential pathogens, especially in low biomass, complex and diverse environmental microbial communities like those in air samples. This limitation is due to a reference database that is strongly biased towards human-associated organisms. Therefore, additional studies and methods can further validate the presence of specific pathogens identified in these air samples. These could include culture-based methods, although their efficacy may be compromised by the low biomass, and targeted qPCR, depending on the availability of species-specific primers.

We observed a trend among pathogens in dusty conditions, indicating increased richness with higher PM_{10} concentrations, although this association did not reach statistical significance (Pearson's correlation, r=0.45, p=0.12). However, we did not find significant correlation between pathogen diversity and dusty conditions (Pearson's correlation, r=0.22, p=0.46). Similarly, we noted a clear pattern suggesting heightened richness and diversity with higher temperatures across all samples (Pearson's correlation, r=0.50, p<0.001 and r=0.48, p<0.001, respectively). This trend was particularly pronounced under clear conditions (r=0.70, p<0.001 and r=0.70, p<0.001, respectively). These findings suggest that under dusty conditions, certain types of potential pathogens are transported, while rising temperatures contribute to this process by adding a diverse range of species rather than specific ones as observed under dusty days.

We examined how dust storms and temperature variations influenced the composition of potential pathogens within the atmospheric microbiome. We found that the abundance ($\log_{10}$(CPM)) of several fungal and bacterial species displayed significant positive correlations with increasing PM_{10} concentrations across all samples. This includes fungal species *Aspergillus fumigatus* (Pearson's correlation, r=0.37, p=0.012), *Aspergillus nidulans* (r=0.36, p=0.015), and *Cercospora beticola* (r=0.34, p=0.021), as well as bacterial species *P. multocida* (r=0.31, p=0.039), all exhibited significant positive correlations with PM_{10} concentrations. To further investigate this relationship while considering potential confounding variables like temperature, we conducted a separate analysis focusing on the correlation between these species and PM_{10} concentrations, specifically during dusty conditions. This analysis revealed a heightened impact of dust storms on certain species. We identified significant positive correlations between bacterial species such as *K. pneumonia* (Pearson's correlation, r=0.60, p=0.030) and *S. maltophilia* (r=0.58, p=0.039), alongside fungal species like *Puccinia striiformis* (r=0.60, p=0.030), and increasing PM_{10} concentrations. Similarly, we found that many species were correlated with temperature, particularly potential fungal pathogens such as *Aspergillus*, *Fusarium*, *Zymoseptoria*, and

bacterial pathogens such as *Acinetobacter* and *Staphylococcus*. These results are depicted in Fig. 2B.

It is important to acknowledge that due to the low abundance of potential pathogenic microorganisms in the atmosphere, detecting significant correlations between these microbial features and environmental variables is challenging. The fluctuations in their abundance in response to environmental factors might not always be statistically evident due to the inherent variability in the atmospheric microbiome. Nevertheless, studying their co-occurrence patterns, as evidenced by significant correlations between specific taxa, can provide valuable insights into potential associations. To gain further insights into the relationship between potential pathogens and dust storms, we explored their associations with dust-signature taxa. These taxa are specific microbial groups linked to dust events, serving as indicators of dusty atmospheric conditions. Within our study, the top five taxa, *G. obscurus* (Pearson's correlation, r=0.51, p<0.001), *Pseudarthrobacter* sp. NS4 (r=0.48, p=0.001), *Rubrobacter marinus* (r=0.48, p=0.001), *Rubrobacter tropicus* (r=0.46, p=0.002), and *Kocuria turfanensis* (r=0.45, p=0.002) exhibited the highest significant correlations with increasing PM_{10} concentrations across all samples, designating them as the dust-indicator species. Further exploration through literature searches revealed that these taxa or their close phylogenetic relatives are frequently encountered in harsh environments such as rock varnish in deserts. Moreover, they possess intriguing phenotypes such as UV-C resistance or resilience to severe desiccation, providing additional support for their association with harsh desert environments (34-36). Remarkably, we found that the dust-indicator taxa displayed robust positive correlations with each other, suggesting their shared association with environmental conditions indicative of dusty atmospheric events. Furthermore, this analysis highlighted that the specific correlations observed between certain groups of taxa and environmental variables such as PM_{10} concentration and temperature were also reflected in their correlations with each other. Co-occurrence patterns offer a clearer reflection of this relationship (Fig. 2C). While we found significant correlations between a few pathogens and PM_{10} concentrations, co-occurrence analysis showed that several pathogens were associated with dust-indicator taxa, suggesting their long-range transport. This observation indicates that certain potential pathogens may share ecological similarities either with dust-indicator taxa or among themselves, suggesting their origins (e.g., deserts) or lifestyle preferences (e.g., temperature effects on microbial growth, leading to changes in composition).

Antimicrobial Resistance and Virulence Profile of the Atmospheric Microbiome

To comprehensively understand the dynamics of specific functions related to antimicrobial resistance and virulence within the atmospheric microbiome, we conducted an extensive analysis. We identified sixty-five distinct Pfam entries associated with antimicrobial resistance showing varying levels of abundance and prevalence across all samples. These entries represent resistance against twenty-four distinct classes of antimicrobials. The normalized abundance of these features in each sample is quantified in reads per kilobase per million mapped reads (RPKM) and presented in Dataset S7. Among the protein families and domains linked to resistance, those associated with multidrug resistance (PF00873, PF01636, PF12802, PF05977, PF01047), bleomycin and fosfomycin resistance (PF00903), tetracycline resistance (PF00440), beta-lactam antibiotics resistance (PF00144, PF00753), and novobiocin and deoxycholate resistance (PF13533) displayed notably higher mean read abundance ($\log_{10}$(RPKM)) and prevalence across all samples compared to other features. These results are illustrated in Fig. S14A. Additionally, several of these features showed a positive correlation with increasing PM_{10} concentrations across all samples, particularly

under dusty atmospheric conditions, as well as with rising temperatures, although to a lesser degree. These findings are depicted in Fig. S14B.

Similarly, we identified one hundred and eighty-one distinct Pfam entries associated with various mechanisms related to virulence and pathogenicity within atmospheric microbiome. These entries exhibited a diverse distribution of abundance and prevalence across all samples. The normalized abundance of these features, measured in RPKM and presented in Dataset S8. Notably, the RmlD substrate binding domain (PF04321), virulence factor BrkB (PF03631), lipid II flippase MurJ (PF03023), and clp amino-terminal domain, a pathogenicity island component (PF02861), displayed significantly higher mean read abundance ($\log_{10}$(RPKM)) and prevalence across all samples compared to other features. These results are presented in Fig. S15A. Some of these features exhibited positive correlations with increasing PM_{10} concentrations and temperature variation across all samples, particularly under dusty atmospheric conditions. These features encompassed various aspects of virulence and pathogenicity, including cell adhesion, motility, biofilm formation, protective immunity and colonization, regulation of genes linked to virulence, stress survival, and pathogenicity-related cellular secretion systems. These findings are depicted in Fig. S15B. Notably, some of these features associated with dust storms, such as the virulence factor BrkB (PF03631), pneumococcal surface protein A (PspA), the aerotolerance regulator N−terminal (PF07584), and temperature, such as the PilZ domain (PF07238) and Clp amino terminal domain (PF02861) are linked to an increased risk of virulence for respiratory diseases in various microbial agents (*37-48*).

We also noticed a trend in the number of contigs associated with antibiotic resistance and virulence (richness) concerning increasing PM_{10} concentration on dusty days and temperature across all samples, particularly on clear days. Additionally, we observed that the diversity of antimicrobial resistance contigs under dusty conditions was higher, indicating a more even distribution with increasing richness. Conversely, the diversity of virulence-associated contigs was lower on clear days compared to dusty days, suggesting the dominance of certain features under dusty conditions (Fig. S16 and S17).

Next, we explored the host microorganisms harboring antibiotic resistance and virulence-related traits by conducting taxonomic assignment to the contigs containing these features. We found that 46.33±5.10% and 52.31±6.99% (mean ± SD) of all antibiotic resistance and virulence-contigs, respectively, did not classify with any level of taxa (Fig. S18 and S19). This suggests either a prevalence of undiscovered species carrying these traits within the atmospheric microbiome or potential limitations in the taxonomic classification algorithm (Kraken2) used, resulting in the failure to identify taxa for these contigs. Additionally, we note that only a negligible fraction of the total antimicrobial resistance and virulence-contigs were associated with potential pathogenic species (Fig. S20 and S21). We then investigated whether this was due to a technical limitation in the read assembly step. Given the low biomass, it is plausible that the DNA fragments of these less abundant species could not find matching overlapping reads. However, our analysis revealed that numerous assembled reads were taxonomically classified to respective pathogenic species (Fig. S22). For example, within only six air samples, a few contigs carrying antimicrobial resistance traits were taxonomically classified as *K. pneumoniae*, a prevalent potential pathogen. These contigs exhibited low abundance (RPKM: 3.78±2.42, mean±SD), whereas the total contig abundance of this species was substantially higher (271.57±218.12) within these samples. However, no virulence genes linked to this species were found in any of the samples. This suggests that these potential pathogens are less likely to carry these genes in the atmospheric

microbiome, and the observed association between these features and PM_{10} and temperature variations was not due to increased pathogen abundance. Moreover, in dusty atmospheric conditions, most of the antimicrobial resistance and virulence-contigs were associated with dust-indicator taxa and other terrestrial taxa, exhibiting increased abundance (RPKM) compared to clear atmospheric day samples (Fig. 4). In contrast, during clear atmospheric conditions, these traits were associated with a diverse array of random taxa.

Discussion

The extensive metagenomic examination of the atmospheric microbiome in the Eastern Mediterranean region has provided valuable insights into microbial dynamics and potential ecological impacts. Our findings reveal a diverse range of potential pathogens relevant to humans, animals, and plants, particularly associated with events of dust transport. For instance, certain bacterial species, such as *K. pneumonia* (*49*), *S. maltophilia* (*50*), and *P. multocida* (*51*) are specifically linked to human respiratory infections such as pneumonia. Fungal species like *A. fumigatus* (*52*), *A. nidulans* (which primarily affects immunocompromised individuals through conidia inhalation) (*53*) and *Aspergillus chevalieri* (with the potential to cause skin infections, notably cutaneous aspergillosis) (*54*) are associated with invasive pulmonary aspergillosis. Additionally, several *Staphylococcus* bacteria, including *Staphylococcus xylosus*, *Staphylococcus equorum*, *Staphylococcus arlettae*, *Staphylococcus cohnii*, and *Staphylococcus saprophyticus*, known to be associated with a range of infections such as bloodstream infections, urinary tract infections, and endocarditis (*55-59*). Moreover, the multi-host plant pathogen *Pseudomonas viridiflava*, with significant implications for agricultural crops such as tomatoes, melons, lettuce, chrysanthemums, and eggplants (*60*), is linked to dust storms. We also observed notable associations between temperature variations and certain potential pathogens, particularly fungi. For instance, *Zymoseptoria tritici*, *Fusarium poae*, and *P. striiformis*, can cause destructive wheat diseases like septoria tritici blotch, fusarium head blight and wheat yellow rust, respectively (*61-63*). Similarly, *C. beticola*, is the causative agent of the most detrimental foliar disease in sugar beet (*64*). In addition, certain potential pathogens associated with human diseases, such as *Aspergillus luchuensis*, known for causing invasive pulmonary aspergillosis (*65*), and *Aspergillus oryzae*, reported to induce peritonitis (*66*), exhibit a positive correlation with rising temperatures.

The observed increasing trends in pathogen richness and compositional changes in abundance suggest a significant association with dust storms and temperature variations. This indicates that dust storms may drive the dispersal of these microorganisms and that certain groups within the atmospheric microbiome may be temperature dependent. As previously discussed, these microorganisms have been reported to cause various human, animal, and plant diseases. Therefore, it is plausible that dust storms and rising temperatures could pose potential threats to human and environmental health. However, drawing a definitive scientific conclusion regarding the immediate public or environmental health implications requires further investigation. The identified microorganisms inhabit diverse primary habitats, including environments such as soil, oceans, humans, and other animals. Many of these pathogens are opportunistic, meaning they typically do not harm their host but can cause diseases, especially when the host's resistance is compromised. Additionally, these pathogens are associated with various diseases beyond those discussed here. For example, while there have been reports of *P. multocida* causing respiratory and other invasive infections, particularly in immunocompromised individuals (*51, 67, 68*), this bacterium commonly causes soft tissue infections following bites or scratches, typically associated with domestic animal injuries (*69*). Furthermore, the pathogenicity of facultative

pathogens is complex. It depends on various factors such as infective dosage, the host's immune status, transmission route, and the presence of other competitive species on the host (*70, 71*). For example, among these variables, the most critical factor is the initial dose of pathogens needed to trigger an infection in individual hosts, referred to as the infective dosage. Although information on infectious doses via inhalation for potential pathogens associated with dust storms and temperature variation in this study is somewhat limited in the literature, previous research employing various experimental models suggests that pathogens like *K. pneumoniae* and *S. maltophilia* tend to have higher infective dosage compared to others such as *Shigella* (*72-75*). Therefore, even if the absolute abundance of these species increases under dusty conditions, as indicated by their rising relative abundance and the overall higher microbial biomass, it may not necessarily imply an immediate potential health or ecological risk. Moreover, although a prior study involving dust samples suggested that some airborne bacteria potentially exhibit biochemical activity (*10*), we lack direct evidence of the viability of these pathogens within the scope of this work. On the other hand, while we noted a significant correlation between dust storms, rising temperatures, and specific antibiotic resistance genes and virulence traits (particularly associated with respiratory diseases) within the atmospheric microbiome, we observed that only a negligible fraction of these species exhibited pathogenic traits within the atmospheric microbiome. This could be attributed to technical limitations associated with low-biomass samples, and these species might still harbor important genes linked to pathogenicity or hypervirulence. Co-assembling similar samples from the same origin might yield different results in this regard, warranting further investigation in future studies. While the presence of pathogenicity traits generally suggests an increased risk of pathogenicity, it is crucial to note that even when these traits are associated with certain pathogens, they are insufficient alone to cause disease.

Notably, we found that most of these genes, particularly on dusty days, were harbored by soil bacteria. This finding is not surprising, considering that soil microbiota represents one of the ancient evolutionary origins of antibiotic resistance and has been proposed as a reservoir of resistance genes (*76*). Although pristine soil microbiomes, such as those found in deserts, contain fewer antibiotic resistance genes compared to non-desert soils (*77*), it is plausible that we observed an increased abundance of these features on dusty days compared to clear days, which lack strong soil influence. Previous studies have reported increased antibiotic resistance gene abundance by qPCR on dusty days, attributing it to anthropogenic influence (*7, 8*). However, our results implicate soil bacteria as the primary source. Regarding virulence genes, it is reasonable to assume that microorganisms typically employ similar strategies to interact with hosts in microbial ecosystems. The emergence of new pathogens is often associated with gene loss or horizontal gene transfer from other species (*78, 79*). For instance, pathogenic strains of *Enterococcus faecium* evolved from commensal species via horizontal gene transfer (*80*). Therefore, it is unsurprising that most virulence factors were connected to non-pathogenic microorganisms in this study. Additionally, some factors, such as those related to colonization, may assist these organisms in thriving in their habitat, thus possessing more generalized functions essential for survival in the environment (*81*).

While the lack of evidence connecting dust-borne pathogens to antimicrobial resistance and virulence-related genes suggests a reduced risk of pathogenicity among these species in the atmospheric microbiome, the dispersal of antimicrobial genes through dust storms could have indirect and long-term ecological consequences. The substantial genetic reservoir present in soil indicates a continuous emergence of new antimicrobial resistance traits in

this environment. Once these genes become mobile within microbial chromosomes, they have the potential to be transferred to pathogens. This transfer may occur within environmental settings or within the microbiota of humans or domestic animals. Even if these genes reside in inactive microbes or as extracellular DNA in air samples, they could still be assimilated into the genomes of viable cells, albeit with relatively low probabilities (*82*). Consequently, the dispersal of these genes through dust storms could facilitate the emergence of new resistance in pathogens across various ecosystems. Therefore, it is crucial to understand whether these genes are already mobile within the atmospheric microbiome, emphasizing the need for further studies in this area.

The atmosphere remains one of the least explored ecosystems concerning microbial characteristics. Consistent with previous studies (*28, 83*), our findings indicate a low fraction of total reads corresponding to taxa, possibly due to undiscovered microorganisms absent from reference databases. Therefore, we cannot exclude the potential bias in our results arising from a database that strongly favors human-associated organisms. For example, databases contain a higher proportion of genomes and antibiotic resistance genes from human and animal pathogens compared to those from commensal or environmental microbes.

Although our findings do not directly indicate immediate public or environmental health threats, there is a clear need for ongoing surveillance to better understand the broader implications of dust storms and temperature rise in the context of escalating climate change on the atmospheric microbiome. The observed connections between dust storms, rising temperatures, and specific pathogens and functions related to pathogenicity emphasize the importance of adopting a comprehensive One Health approach in response to global climate shifts. By recognizing the interconnectedness of human, animal, and environmental health, we can develop comprehensive and interdisciplinary strategies to effectively anticipate and mitigate the risks posed by airborne microorganisms to public health and ecology. This approach is a vital component in strengthening global health security and safeguarding the well-being of all organisms within the ever-changing climate framework.

Materials and Methods

Sample collection

We collected air samples on the rooftop of a four-story building at the Weizmann Institute of Science in Rehovot, Israel (31.9070 N, 34.8102 E; 80 m above mean sea level). During a specific 64-day period from the end of March to the close of May 2022, we collected a total of 45 air samples. This timeframe allowed us to capture the diverse dynamics of air masses affected by distinct Eastern and Western dust storm origins, as well as the fluctuations in temperature ranging from 16.5 to 27.1 °C. To ensure an effective sampling design, we utilized various atmospheric forecast platforms (details can be found in the Supplementary Materials). We verified the accuracy of dust storm predictions by cross-referencing them with PM_{10} data obtained from the Rehovot Air Monitoring station of the Israeli Ministry of Environmental Protection (https://air.sviva.gov.il/). To mitigate potential confounding effect of the diel cycle of the atmospheric microbiome (*28*), we collected all samples specifically from 9:00 to 12:00. We chose this time frame to minimize variations in microbial composition and activity throughout the day. However, in cases where dust forecasts indicated a dust storm or other significant atmospheric events outside this time slot, we adjusted sample collection accordingly to ensure representative sampling.

For metagenomics analysis, we employed the Coriolis μ microbial air sampler (Bertin Technologies) to collect air samples for 2 hours, at a flow rate of 200 L/min. This impinger captures particles larger than 0.5 μm, with a collection efficiency with a D_{50} value, denoting the particle size at which the collection efficiency reaches 50%, exceeding 0.5 μm. During collection, samples were stored in 15 ml of a nucleic acids preservation solution to maintain sample integrity (10), and measures were taken to minimize evaporation by supplementing the samples with a top-off-flow rate of 0.5-1.5 ml per minute of molecular grade water. Before each sampling event, we thoroughly decontaminate the Coriolis sampler as described in the Supplementary Materials. Following collection, we concentrated the sample onto autoclaved and sterilized polyethersulfone (PES) filters (diameter of 25 mm and a pore size of 0.1 μm (Sartorius Stedim Biotech)) using a sterile single-use syringe and reusable syringe filter holders (Sartorius Stedim Biotech). Then, we transferred the filter samples into Falcon tubes and stored at -20°C for preservation. We conducted DNA extraction from the filters within 2-3 days after collection to ensure optimal sample quality. To generate operating blanks, we replicated the same procedure, but we operated the sampler for 5 seconds. Consequently, we obtained a total of seven operating blanks on randomly selected dates before the actual sample collection process. This ensured the capture of background environmental conditions and potential contamination present in the sampling setup. Further details regarding the DNA yield, shotgun metagenome, and taxonomic classification results obtained from control samples can be found in the Supplementary Materials.

Collection of meteorological data and dust column density maps

We collected data on particulate matter concentration (PM, μg m^{-3}), temperature (T, °C), relative humidity (RH, %), and rain (mm) from the Rehovot Air Monitoring station, located approximately 1 km from the sampling site. This station is part of the Israeli Ministry of Environmental Protection network. Meteorological data were recorded in 5-min time intervals. To estimate the origin of the dust, we acquired time-averaged maps of dust column mass density (at a 0.5° × 0.625° resolution) and reanalysis meteorological data from the Modern-Era Retrospective analysis for Research and Applications (MERRA-2) for each sampling event. For each event, we performed a retrospective analysis using the Giovanni online data system, developed and maintained by the NASA GES DISC (*84*), by using hourly frames of dust column density maps 72 hours prior to the sampling event. These frames were compiled into dust column density map movies using the 'av' package in R, with data at 6-hour intervals. Additionally, we investigated the origin of the air mass with the Hybrid Single-Particle Lagrangian Integrated Trajectory model (HYSPLIT) (https://www.ready.noaa.gov/index.php/) (*85, 86*). For each analysis, we calculated a 72-hour back trajectory at three distinct altitudes (0, 50, and 100 meters above ground level).

DNA Extraction

We extracted DNA from the filters using a PowerWater DNA isolation kit (Qiagen, Dresden, Germany) following the manufacturer's protocol. Following this, we quantified the extracted DNA from the samples using a Qubit 2.0 fluorometer, employing the Qubit dsDNA HS (High Sensitivity) Assay Kit (Invitrogen) with dsDNA HS buffer. Detailed information regarding the DNA yield obtained from the control samples can be found in the Supplementary Materials.

DNA Library Preparation and Metagenomic Sequencing

Shotgun metagenome libraries were generated using a Nextera XT library preparation kit according to the manufacturer's instructions (Illumina). The libraries were pooled and sequenced using high-output flow cells with paired-end 2 × 150 base reads on an Illumina

NovaSeq6000 sequencer, utilizing an S4 flow cell. The library preparation and sequencing processes were conducted at the Rush Genomics and Microbiome Core Facility (GMCF) located at Rush University.

Data processing and metagenomic analysis

We performed a comprehensive quality assessment of the metagenomic datasets using FASTQC software (version 0.11.9, www.bioinformatics.babraham.ac.uk/projects/fastqc/). We applied quality trimming and Illumina adapter removal using Trimmomatic (*87*) with specific parameters: ILLUMINACLIP:TruSeq3-PE.fa:2:30:10 LEADING:20, TRAILING:20, SLIDINGWINDOW:4:15, and MINLEN:35. The application of Trimmomatic's quality control steps resulted in an average of 4.3 million high-quality reads per sample (3-11 million paired-end) that met the predefined quality criteria, as presented in Datasets S9 and S10.

We performed taxonomic classification of the metagenomic data using Kraken2 (v2.1.2), which employs exact k-mer matching directly on paired reads (--paired --minimum-hit-groups 10 --confidence 0.1) (*88*). In this procedure, we constructed a custom database of taxa-specific k-mers using complete reference genomes/proteins from diverse taxonomic groups, including archaea, bacteria, viruses, fungi, and protozoa, sourced from the NCBI RefSeq database on January 22, 2023 (kraken2-build --build). Before constructing the database, we masked repetitive regions in reference genomes using Dustmasker to prevent false positives in the results (*89*). Subsequently, we applied Bracken (v2.7.0) to further refine the outcomes (*90*). For this, we constructed Bracken databases using the options (-k 35 -l 150). The re-estimation of taxa abundance was specifically conducted at the species level, with a minimum threshold of 10 counts to ensure sufficient confidence in the assigned taxonomic classification. If the re-estimation extends to another classification level (e.g., genus, family, order, or phylum), the threshold for abundance estimation will be applied at that level. To evaluate Kraken's classification accuracy and differentiate between reads distributed throughout a reference genome and those associated with only a small segment (potentially indicating false positives), we estimated the number of distinct k-mers linked to each taxon in the input sequencing data using KrakenUniq (*91*). This functionality is integrated within the Kraken2 algorithm by configuring the relevant options (--report-minimizer-data).

To further assess the specificity of taxonomic classification result, we conducted read mapping from each sample to reference genomes, focusing particularly on low-abundance species such as potential pathogens detected in air samples. We obtained the reference genomes of the thirty-four most prevalent potential pathogens, and generally the most abundant taxa across all samples, with *G. obscurus* as a reference, from the NCBI RefSeq database on February 12, 2024. Subsequently, we aligned all reads from the samples to each reference genome separately using Bowtie2 (--very-sensitive-local) (*92*). The mapping results of each individual sample were sorted and converted to BAM format using SAMtools (*93*). We reported genome coverage for all positions and the fractions of genome covered by reads using the bedtools genomecov command (-bga) and (-max 50), respectively (*94*). Finally, we visualized genome tracks using the 'circlize' package in R (*95*).

We performed functional profiling of the metagenomics data using the BLASTX function in DIAMOND (v2.1.7.161) (*96*), utilizing merged paired-end reads and specific parameters (--very-sensitive --id 80 --query-cover 80) to enhance sensitivity. For this analysis, we

employed the NCBI-nr database from June 2023. Subsequently, we processed the DIAMOND results further using the daa-meganizer tool (--minScore 80 --minPercentIdentity 80 --minSupport 5) in MEGAN (version 6.24.20) (*97*). Functional features were assigned if there were at least 5 reads that uniquely aligned with a specific feature. To annotate the NCBI-nr data into SEED categories, we utilized the megan-map-Feb2022.db file.

We conducted metagenomic assembly using metaSPAdes (version 3.15.3) (*98*) on quality-trimmed, paired-end reads, employing default settings. Prediction of open reading frames (ORFs) for protein-coding genes from assembled contigs was achieved using Prodigal (version 2.6.3) (*99*) with the '-p meta' option, enabling anonymous mode as recommended for metagenomic datasets.

We carried out antimicrobial resistance and virulence profiling of the metagenomic data using hmmscan (HMMER, version 3.3.2-gompic-2020b) (*100*) with a stringent e-value threshold of 1×10^{-5} to predict the function of Open Reading Frames (ORFs). Separate searches were performed for genes containing Pfam modules (*101*) related to 'antibiotic resistance', 'virulence', and 'pathogenicity'. We retained only the top matches in the hmmscan results when the same ORFs yielded multiple hits to the same Pfam entry or the same contig had more than one hit, which was rare due to short contig lengths.

To estimate the abundance of all contigs, including those associated with antimicrobial resistance and virulence, we mapped the quality-trimmed, paired-end reads to the contigs in each sample, providing coverage information. This mapping was performed using bbmap.sh (BBMap, v.38.90) with default settings. Subsequently, we utilized pileup.sh to convert the coverage data into reads per kilobase per million mapped reads (RPKM). This normalization procedure ensures accurate rescaling to correct for both library size and gene length. We then conducted taxonomic annotation on these contigs using Kraken2 with default parameters, employing the same custom database constructed from diverse taxonomic groups, as discussed previously. The complete lineage of taxonomy was obtained for each contig from the kingdom level to the species level using Taxonkit with the taxdump file downloaded from the NCBI database on February 27, 2024 (*102*). Sankey diagram was created using the 'networkD3' package in R for visualization.

Statistical Analysis

To address variations in library size across samples, we normalized the read counts obtained from tools such as Bracken and DIAMOND to counts per million (CPM) values. This normalization was performed by calculating CPM values, where each value represents the relative proportion of reads (i.e., reads normalized for library size through total sum scaling) multiplied by 1,000,000. Our metagenomics data deviated from the fundamental assumption that most features should exhibit minimal changes between samples. Consequently, we refrained from employing alternative inter-sampling normalization approaches. Instead, we opted for CPM normalization as it adequately accounts for library size differences and facilitates reliable comparisons of read abundances across samples.

We computed the richness (observed number of features) and Shannon–Wiener diversity index, which assesses the uncertainty related to predicting the identity of a randomly chosen individual within the community, for both taxonomic and functional features using the R package 'vegan'. To explore the connections between composition, richness, diversity of taxonomic and functional features, and environmental factors (such as daily mean PM_{10}

concentration, temperature, and relative humidity), we conducted Pearson's correlation analysis. This analysis was performed using the R package 'Hmisc'.

Principal Coordinates Analysis (PCoA) was used as the ordination method based on Bray–Curtis dissimilarity of taxonomic and functional compositional data (i.e., relative taxa or functional feature abundance, calculated as the reads assigned to a taxa or function divided by the sum), and this analysis was conducted using the R package 'vegan'. The heatmap representing the Bray–Curtis dissimilarity of taxonomic and functional compositional data was visualized using the R package 'ComplexHeatmap'.

We applied a filtering criterion to focus our analysis on taxonomic and functional features with a significant presence in the dataset (details can be found in the Supplementary Materials).

We used the Shapiro–Wilk normality test to assess data distribution normality. The test results indicated a failure to meet this assumption. Therefore, we chose a nonparametric method for comparing the two groups. The Wilcoxon rank sum test, also known as the Mann–Whitney *U* test, was utilized to assess the differential relative abundance of taxa between the dusty and clear atmospheric conditions. To account for multiple comparisons, we applied the Benjamini–Hochberg correction to control for false discovery rate, with the adjusted P-value below 0.05 indicating statistical significance.

We assessed the relationship between specific microbial features (abundance of species and contigs associated with antimicrobial resistance, virulence, and pathogenicity) and environmental variables (including daily mean PM_{10} concentration and temperature) using Pearson's correlation. A statistically significant correlation was considered for an absolute Pearson's correlation coefficient (r) value above 0.3 and a P-value below 0.05. The rationale for this analysis is detailed in the Supplementary Materials.

We conducted a co-occurrence analysis of microbial species based on Pearson's correlation to explore the relationship between specific taxa. Only results meeting the following criteria were considered statistically robust between taxa and retained for further examination: an absolute Pearson's correlation coefficient (r) value above 0.3 and a P-value below 0.05, after adjustment by Benjamini–Hochberg's method to reduce the chances of obtaining false-positive results.

We performed an ANOVA analysis using distance matrices to assess the extent to which the variation in the composition of the atmospheric microbiome (i.e., both taxonomic and functional features) could be attributed to individual variables. For this analysis, we employed the Adonis2 function from the 'vegan' package, which performs permutational MANOVA, utilizing 1000 permutations and the Bray–Curtis dissimilarity matrix of taxonomic and functional compositional data (i.e., relative abundance). The following formula design was employed: daily mean PM_{10} + air mass origin + daily mean relative humidity + daily mean temperature, in the specified order. Significance was determined based on a threshold of P-value below 0.05. Furthermore, we assessed the differences in the composition of the atmospheric microbiome between dusty and clear atmospheric conditions using the same methodology. To evaluate the multivariate homogeneity of group dispersions, an assumption of MANOVA, we employed the Betadisper function with 1000 permutations.

For detailed descriptions of the methods and further relevant information, please refer to the Supplementary Materials.

References

1. J. Fröhlich-Nowoisky *et al.*, Bioaerosols in the Earth system: Climate, health, and ecosystem interactions. *Atmospheric Research* **182**, 346-376 (2016).
2. L. N. Kobziar *et al.*, Wildland fire smoke alters the composition, diversity, and potential atmospheric function of microbial life in the aerobiome. *ISME Commun* **2**, 8 (2022).
3. Y. S. Joung, Z. Ge, C. R. Buie, Bioaerosol generation by raindrops on soil. *Nat Commun* **8**, 14668 (2017).
4. J. M. Michaud *et al.*, Taxon-specific aerosolization of bacteria and viruses in an experimental ocean-atmosphere mesocosm. *Nat Commun* **9**, 2017 (2018).
5. G. Varga, G. Újvári, J. Kovács, Spatiotemporal patterns of Saharan dust outbreaks in the Mediterranean Basin. *Aeolian Research* **15**, 151-160 (2014).
6. S. Bodenheimer, I. M. Lensky, U. Dayan, Characterization of Eastern Mediterranean dust storms by area of origin; North Africa vs. Arabian Peninsula. *Atmospheric Environment* **198**, 158-165 (2019).
7. Y. Mazar, E. Cytryn, Y. Erel, Y. Rudich, Effect of Dust Storms on the Atmospheric Microbiome in the Eastern Mediterranean. *Environ Sci Technol* **50**, 4194-4202 (2016).
8. D. Gat, Y. Mazar, E. Cytryn, Y. Rudich, Origin-Dependent Variations in the Atmospheric Microbiome Community in Eastern Mediterranean Dust Storms. *Environ Sci Technol* **51**, 6709-6718 (2017).
9. E. Mayol *et al.*, Long-range transport of airborne microbes over the global tropical and subtropical ocean. *Nat Commun* **8**, 201 (2017).
10. B. A. Erkorkmaz, D. Gat, Y. Rudich, Aerial transport of bacteria by dust plumes in the Eastern Mediterranean revealed by complementary rRNA/rRNA-gene sequencing. *Communications Earth & Environment* **4**, 24 (2023).
11. E. Rahav, G. Ovadia, A. Paytan, B. Herut, Contribution of airborne microbes to bacterial production and N2 fixation in seawater upon aerosol deposition. *Geophysical Research Letters* **43**, 719-727 (2016).
12. C. Guo *et al.*, Shifts in Microbial Community Structure and Activity in the Ultra-Oligotrophic Eastern Mediterranean Sea Driven by the Deposition of Saharan Dust and European Aerosols. *Frontiers in Marine Science* **3**, (2016).
13. N. Lang-Yona *et al.*, Annual distribution of allergenic fungal spores in atmospheric particulate matter in the Eastern Mediterranean; a comparative study between ergosterol and quantitative PCR analysis. *Atmospheric Chemistry and Physics* **12**, 2681-2690 (2012).
14. H. Brodsky *et al.*, Assessing long-distance atmospheric transport of soilborne plant pathogens. *Environ Res Lett* **18**, (2023).
15. C. Gonzalez-Martin, N. Teigell-Perez, B. Valladares, D. W. Griffin, The Global Dispersion of Pathogenic Microorganisms by Dust Storms and Its Relevance to Agriculture. *Adv Agron* **127**, 1-41 (2014).
16. J. Rotem, Sand and dust storms as factors leading to alternaria blight epidemics on potatoes and tomatoes. *Agricultural Meteorology* **2**, 281-288 (1965).
17. C. Zhang *et al.*, Mortality risks from a spectrum of causes associated with sand and dust storms in China. *Nature Communications* **14**, 6867 (2023).
18. S. Z. Sajani *et al.*, Saharan dust and daily mortality in Emilia-Romagna (Italy). *Occupational and Environmental Medicine* **68**, 446-451 (2011).
19. Z. Meng, B. Lu, Dust events as a risk factor for daily hospitalization for respiratory and cardiovascular diseases in Minqin, China. *Atmospheric Environment* **41**, 7048-7058 (2007).

20. C.-C. Chan, H.-C. Ng, A case-crossover analysis of Asian dust storms and mortality in the downwind areas using 14-year data in Taipei. *Science of The Total Environment* **410-411**, 47-52 (2011).
21. W. W. S. TAM, T. W. WONG, A. H. S. WONG, D. S. C. HUI, Effect of dust storm events on daily emergency admissions for respiratory diseases. *Respirology* **17**, 143-148 (2012).
22. A. Vodonos *et al.*, The impact of desert dust exposures on hospitalizations due to exacerbation of chronic obstructive pulmonary disease. *Air Quality, Atmosphere & Health* **7**, 433-439 (2014).
23. C. Lorentzou *et al.*, Extreme desert dust storms and COPD morbidity on the island of Crete. *Int J Chron Obstruct Pulmon Dis* **14**, 1763-1768 (2019).
24. G. Zittis *et al.*, Climate Change and Weather Extremes in the Eastern Mediterranean and Middle East. *Reviews of Geophysics* **60**, e2021RG000762 (2022).
25. T. Ozturk, M. T. Turp, M. Türkeş, M. L. Kurnaz, Future projections of temperature and precipitation climatology for CORDEX-MENA domain using RegCM4.4. *Atmospheric Research* **206**, 87-107 (2018).
26. I. Luhung *et al.*, Experimental parameters defining ultra-low biomass bioaerosol analysis. *NPJ Biofilms Microbiomes* **7**, 37 (2021).
27. D. Gat *et al.*, Size-Resolved Community Structure of Bacteria and Fungi Transported by Dust in the Middle East. *Front Microbiol* **12**, 744117 (2021).
28. E. S. Gusareva *et al.*, Microbial communities in the tropical air ecosystem follow a precise diel cycle. *Proc Natl Acad Sci U S A* **116**, 23299-23308 (2019).
29. P. Amato *et al.*, Metatranscriptomic exploration of microbial functioning in clouds. *Sci Rep* **9**, 4383 (2019).
30. D. Gat, R. Zimmermann, Y. Rudich, Functional Genes Profile of Atmospheric Dust in the East Mediterranean Suggests Widespread Anthropogenic Influence on Aerobiome Composition. *Journal of Geophysical Research: Biogeosciences* **127**, e2022JG007022 (2022).
31. X. Peng, D. Gat, A. Paytan, Y. Rudich, The Response of Airborne Mycobiome to Dust Storms in the Eastern Mediterranean. *Journal of Fungi* **7**, 802 (2021).
32. R. Sarafian, D. Nissenbaum, S. Raveh-Rubin, V. Agrawal, Y. Rudich, Deep multi-task learning for early warnings of dust events implemented for the Middle East. *npj Climate and Atmospheric Science* **6**, 23 (2023).
33. F. U. Battistuzzi, S. B. Hedges, A major clade of prokaryotes with ancient adaptations to life on land. *Mol Biol Evol* **26**, 335-343 (2009).
34. N. Ivanova *et al.*, Complete genome sequence of Geodermatophilus obscurus type strain (G-20). *Stand Genomic Sci* **2**, 158-167 (2010).
35. R. W. Chen *et al.*, Rubrobacter tropicus sp. nov. and Rubrobacter marinus sp. nov., isolated from deep-sea sediment of the South China Sea. *Int J Syst Evol Microbiol* **70**, 5576-5585 (2020).
36. G. Zhou *et al.*, Kocuria flava sp. nov. and Kocuria turfanensis sp. nov., airborne actinobacteria isolated from Xinjiang, China. *Int J Syst Evol Microbiol* **58**, 1304-1307 (2008).
37. R. C. Fernandez, A. A. Weiss, Cloning and sequencing of a Bordetella pertussis serum resistance locus. *Infect Immun* **62**, 4727-4738 (1994).
38. T. L. McCool, T. R. Cate, G. Moy, J. N. Weiser, The immune response to pneumococcal proteins during experimental human carriage. *J Exp Med* **195**, 359-365 (2002).
39. R. Mukerji *et al.*, Pneumococcal surface protein A inhibits complement deposition on the pneumococcal surface by competing with the binding of C-reactive protein to cell-surface phosphocholine. *J Immunol* **189**, 5327-5335 (2012).

40. S. S. Park *et al.*, Streptococcus pneumoniae Binds to Host Lactate Dehydrogenase via PspA and PspC To Enhance Virulence. *mBio* **12**, 10.1128/mbio.00673-00621 (2021).
41. E. R. Lafontaine *et al.*, The autotransporter protein BatA is a protective antigen against lethal aerosol infection with Burkholderia mallei and Burkholderia pseudomallei. *Vaccine X* **1**, 100002 (2019).
42. H. Yesilkaya, V. F. Andisi, P. W. Andrew, J. J. Bijlsma, Streptococcus pneumoniae and reactive oxygen species: an unusual approach to living with radicals. *Trends Microbiol* **21**, 187-195 (2013).
43. M. A. Schumacher, W. Zeng, Structures of the activator of K. pneumonia biofilm formation, MrkH, indicates PilZ domains involved in c-di-GMP and DNA binding. *Proc Natl Acad Sci U S A* **113**, 10067-10072 (2016).
44. J. J. Wilksch *et al.*, MrkH, a novel c-di-GMP-dependent transcriptional activator, controls Klebsiella pneumoniae biofilm formation by regulating type 3 fimbriae expression. *PLoS Pathog* **7**, e1002204 (2011).
45. J. Porankiewicz, J. Wang, A. K. Clarke, New insights into the ATP-dependent Clp protease: Escherichia coli and beyond. *Mol Microbiol* **32**, 449-458 (1999).
46. T. R. Kannan, O. Musatovova, P. Gowda, J. B. Baseman, Characterization of a unique ClpB protein of Mycoplasma pneumoniae and its impact on growth. *Infect Immun* **76**, 5082-5092 (2008).
47. P. Tripathi, L. K. Singh, S. Kumari, O. R. Hakiem, J. K. Batra, ClpB is an essential stress regulator of Mycobacterium tuberculosis and endows survival advantage to dormant bacilli. *Int J Med Microbiol* **310**, 151402 (2020).
48. D. Frees *et al.*, Clp ATPases are required for stress tolerance, intracellular replication and biofilm formation in Staphylococcus aureus. *Mol Microbiol* **54**, 1445-1462 (2004).
49. K. E. Holt *et al.*, Genomic analysis of diversity, population structure, virulence, and antimicrobial resistance in Klebsiella pneumoniae, an urgent threat to public health. *Proc Natl Acad Sci U S A* **112**, E3574-3581 (2015).
50. J. S. Brooke, Stenotrophomonas maltophilia: an emerging global opportunistic pathogen. *Clin Microbiol Rev* **25**, 2-41 (2012).
51. S. Pak, D. Valencia, J. Decker, V. Valencia, Y. Askaroglu, Pasteurella multocida pneumonia in an immunocompetent patient: Case report and systematic review of literature. *Lung India* **35**, 237-240 (2018).
52. M. Kousha, R. Tadi, A. O. Soubani, Pulmonary aspergillosis: a clinical review. *Eur Respir Rev* **20**, 156-174 (2011).
53. R. W. Bastos *et al.*, Functional Characterization of Clinical Isolates of the Opportunistic Fungal Pathogen Aspergillus nidulans. *mSphere* **5**, 10.1128/msphere.00153-00120 (2020).
54. J. Naidu, S. M. Singh, Aspergillus chevalieri (Mangin) Thom and Church: a new opportunistic pathogen of human cutaneous aspergillosis. *Mycoses* **37**, 271-274 (1994).
55. N. Giordano *et al.*, Erythema nodosum associated with Staphylococcus xylosus septicemia. *J Microbiol Immunol Infect* **49**, 134-137 (2016).
56. D. Novakova *et al.*, Staphylococcus equorum and Staphylococcus succinus isolated from human clinical specimens. *J Med Microbiol* **55**, 523-528 (2006).
57. A. Lavecchia *et al.*, Staphylococcus arlettae Genomics: Novel Insights on Candidate Antibiotic Resistance and Virulence Genes in an Emerging Opportunistic Pathogen. *Microorganisms* **7**, (2019).
58. J. C. Motta, C. Forero-Carreno, A. Arango, M. Sanchez, Staphylococcus cohnii endocarditis in native valve. *New Microbes New Infect* **38**, 100825 (2020).
59. J. Hur *et al.*, Staphylococcus saprophyticus Bacteremia originating from Urinary Tract Infections: A Case Report and Literature Review. *Infect Chemother* **48**, 136-139 (2016).

60. P. F. Sarris, E. A. Trantas, E. Mpalantinaki, F. Ververidis, D. E. Goumas, Pseudomonas viridiflava, a multi host plant pathogen with significant genetic variation at the molecular level. *PLoS One* **7**, e36090 (2012).
61. H. Fones, S. Gurr, The impact of Septoria tritici Blotch disease on wheat: An EU perspective. *Fungal Genet Biol* **79**, 3-7 (2015).
62. X. M. Xu *et al.*, Predominance and association of pathogenic fungi causing Fusarium ear blightin wheat in four European countries. *European Journal of Plant Pathology* **112**, 143-154 (2005).
63. W. Chen, C. Wellings, X. Chen, Z. Kang, T. Liu, Wheat stripe (yellow) rust caused by Puccinia striiformis f. sp. tritici. *Mol Plant Pathol* **15**, 433-446 (2014).
64. L. I. Rangel *et al.*, Cercospora beticola: The intoxicating lifestyle of the leaf spot pathogen of sugar beet. *Mol Plant Pathol* **21**, 1020-1041 (2020).
65. Q. Wang *et al.*, Triazole-resistant Aspergillus luchuensis, an industrially important black Aspergillus spp. used in fermentation in East Asia, isolated from the patient with invasive pulmonary aspergillosis in China. *Emerg Microbes Infect* **11**, 1435-1438 (2022).
66. I. Schwetz *et al.*, Aspergillus oryzae peritonitis in CAPD: case report and review of the literature. *Am J Kidney Dis* **49**, 701-704 (2007).
67. S. Yadav, A Case of Pneumonia Caused by Pasteurella multocida in an Immunocompetent Indian Male. *Cureus* **14**, e28820 (2022).
68. D. P. Kofteridis *et al.*, Bacteremic community-acquired pneumonia due to Pasteurella multocida. *International Journal of Infectious Diseases* **13**, e81-e83 (2009).
69. B. A. Wilson, M. Ho, Pasteurella multocida: from zoonosis to cellular microbiology. *Clin Microbiol Rev* **26**, 631-655 (2013).
70. E. C. Keen, Paradigms of pathogenesis: targeting the mobile genetic elements of disease. *Front Cell Infect Microbiol* **2**, 161 (2012).
71. J. Fierer, D. Looney, J.-C. Pechère, in *Infectious Diseases (Fourth Edition),* J. Cohen, W. G. Powderly, S. M. Opal, Eds. (Elsevier, 2017), pp. 4-25.e21.
72. J. Malina, J. Hofmann, J. Franěk, Informative value of a mouse model of Klebsiella pneumoniae infection used as a host-resistance assay. *Folia Microbiol (Praha)* **36**, 183-191 (1991).
73. M. S. Lawlor, J. Hsu, P. D. Rick, V. L. Miller, Identification of Klebsiella pneumoniae virulence determinants using an intranasal infection model. *Molecular Microbiology* **58**, 1054-1073 (2005).
74. A. Pompilio *et al.*, Stenotrophomonas maltophilia Phenotypic and Genotypic Diversity during a 10-year Colonization in the Lungs of a Cystic Fibrosis Patient. *Frontiers in Microbiology* **7**, (2016).
75. H. L. DuPont, M. M. Levine, R. B. Hornick, S. B. Formal, Inoculum size in shigellosis and implications for expected mode of transmission. *J Infect Dis* **159**, 1126-1128 (1989).
76. K. J. Forsberg *et al.*, The Shared Antibiotic Resistome of Soil Bacteria and Human Pathogens. *Science* **337**, 1107-1111 (2012).
77. N. Fierer *et al.*, Cross-biome metagenomic analyses of soil microbial communities and their functional attributes. *Proceedings of the National Academy of Sciences* **109**, 21390-21395 (2012).
78. M. J. Pallen, B. W. Wren, Bacterial pathogenomics. *Nature* **449**, 835-842 (2007).
79. N. F. Brown, M. E. Wickham, B. K. Coombes, B. B. Finlay, Crossing the line: selection and evolution of virulence traits. *PLoS Pathog* **2**, e42 (2006).
80. H. L. Leavis *et al.*, Insertion Sequence–Driven Diversification Creates a Globally Dispersed Emerging Multiresistant Subspecies of E. faecium. *PLOS Pathogens* **3**, e7 (2007).

81. C. Niu *et al.*, Common and pathogen-specific virulence factors are different in function and structure. *Virulence* **4**, 473-482 (2013).
82. D. G. J. Larsson, C.-F. Flach, Antibiotic resistance in the environment. *Nature Reviews Microbiology* **20**, 257-269 (2022).
83. D. I. Drautz-Moses *et al.*, Vertical stratification of the air microbiome in the lower troposphere. *Proceedings of the National Academy of Sciences* **119**, e2117293119 (2022).
84. J. G. Acker, G. Leptoukh, Online analysis enhances use of NASA Earth science data. *Eos, Transactions American Geophysical Union* **88**, 14-17 (2007).
85. M. D. Cohen *et al.*, NOAA's HYSPLIT Atmospheric Transport and Dispersion Modeling System. *Bulletin of the American Meteorological Society* **96**, 2059-2077 (2015).
86. G. Rolph, A. Stein, B. Stunder, Real-time Environmental Applications and Display sYstem: READY. *Environmental Modelling & Software* **95**, 210-228 (2017).
87. A. M. Bolger, M. Lohse, B. Usadel, Trimmomatic: a flexible trimmer for Illumina sequence data. *Bioinformatics* **30**, 2114-2120 (2014).
88. D. E. Wood, J. Lu, B. Langmead, Improved metagenomic analysis with Kraken 2. *Genome Biol* **20**, 257 (2019).
89. A. Morgulis, E. M. Gertz, A. A. Schäffer, R. Agarwala, A fast and symmetric DUST implementation to mask low-complexity DNA sequences. *J Comput Biol* **13**, 1028-1040 (2006).
90. J. Lu, F. P. Breitwieser, P. Thielen, S. L. Salzberg, Bracken: estimating species abundance in metagenomics data. *Peerj Comput Sci* **3**, (2017).
91. F. P. Breitwieser, D. N. Baker, S. L. Salzberg, KrakenUniq: confident and fast metagenomics classification using unique k-mer counts. *Genome Biol* **19**, 198 (2018).
92. B. Langmead, S. L. Salzberg, Fast gapped-read alignment with Bowtie 2. *Nature Methods* **9**, 357-359 (2012).
93. P. Danecek *et al.*, Twelve years of SAMtools and BCFtools. *GigaScience* **10**, (2021).
94. A. R. Quinlan, I. M. Hall, BEDTools: a flexible suite of utilities for comparing genomic features. *Bioinformatics* **26**, 841-842 (2010).
95. Z. Gu, L. Gu, R. Eils, M. Schlesner, B. Brors, circlize implements and enhances circular visualization in R. *Bioinformatics* **30**, 2811-2812 (2014).
96. B. Buchfink, C. Xie, D. H. Huson, Fast and sensitive protein alignment using DIAMOND. *Nat Methods* **12**, 59-60 (2015).
97. D. H. Huson, A. F. Auch, J. Qi, S. C. Schuster, MEGAN analysis of metagenomic data. *Genome Res* **17**, 377-386 (2007).
98. S. Nurk, D. Meleshko, A. Korobeynikov, P. A. Pevzner, metaSPAdes: a new versatile metagenomic assembler. *Genome Res* **27**, 824-834 (2017).
99. D. Hyatt *et al.*, Prodigal: prokaryotic gene recognition and translation initiation site identification. *BMC Bioinformatics* **11**, 119 (2010).
100. S. R. Eddy, A new generation of homology search tools based on probabilistic inference. *Genome Inform* **23**, 205-211 (2009).
101. J. Mistry *et al.*, Pfam: The protein families database in 2021. *Nucleic Acids Res* **49**, D412-D419 (2021).
102. W. Shen, H. Ren, TaxonKit: A practical and efficient NCBI taxonomy toolkit. *Journal of Genetics and Genomics* **48**, 844-850 (2021).

Acknowledgments

Funding:
Weizmann Institute of Science Sustainability and Energy Research Initiative (SAERI)
The de Botton Center for Marine Science

Author contributions:
BAE and YR conceptualized and designed the study, BAE collected air samples, extracted the DNA, and prepared them for sequencing. BAE conducted bioinformatics and data analysis, interpreted, and visualized the results, and drafted the manuscript. BAE and DZ jointly crafted the bioinformatics study design. YR and DZ contributed to reviewing and editing the manuscript. All authors actively participated in result discussions and approved the final manuscript.

Competing interests:
Authors declare that they have no competing interests.

Data and materials availability:
The metagenomic sequences utilized in this study have been deposited in the National Center for Biotechnology Information (NCBI) database under the accession number PRJNA1045528. Additionally, Supplementary Materials, Dataset S5, has been archived in a suitable repository, accessible at (https://doi.org/10.5281/zenodo.11090298).

Figures and Tables

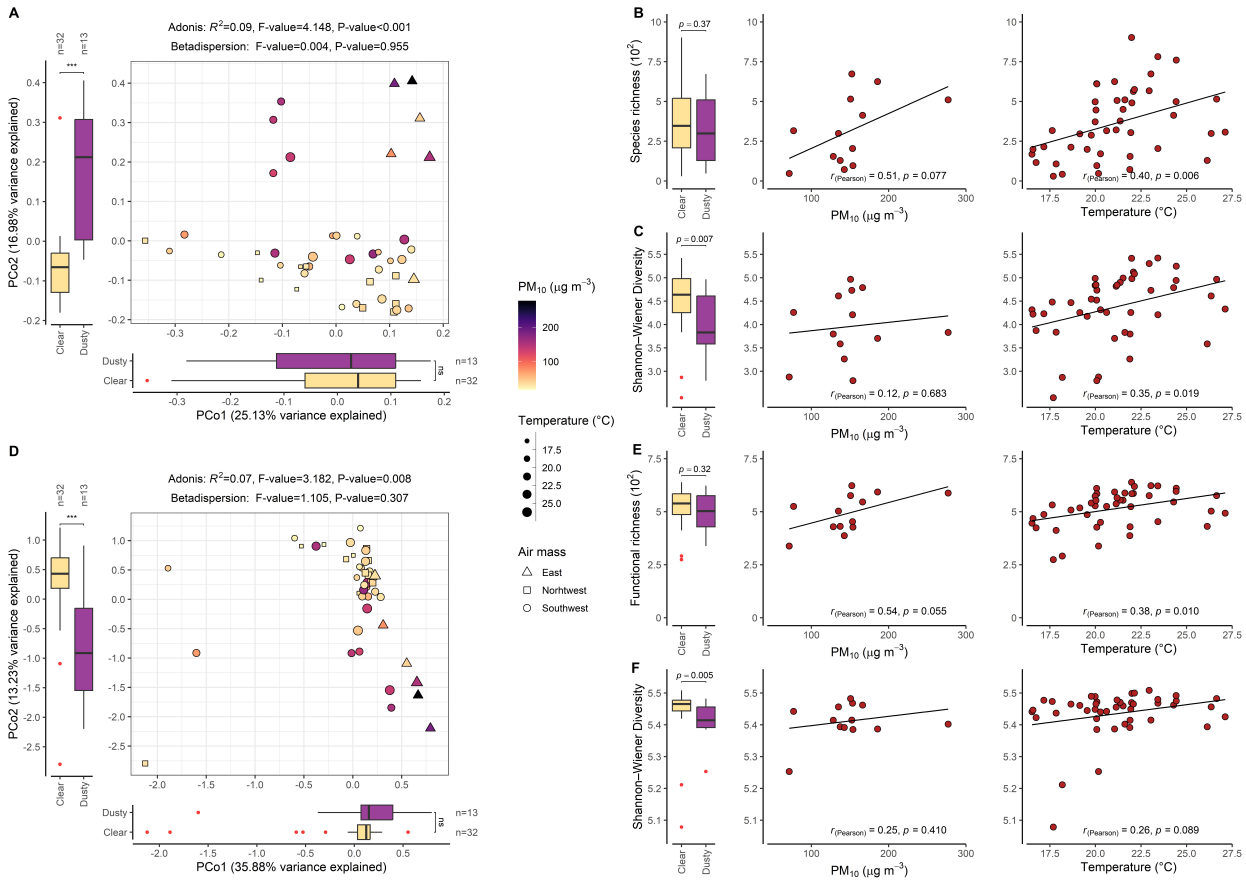

Fig. 1. Taxonomic and functional characteristics of the atmospheric microbiome in relation to environmental variables. (**A**, **D**) Principal Coordinate Analysis (PCoA) plots illustrate Bray–Curtis dissimilarity of taxonomic (**A**) and functional (**D**) features, demonstrating the impact of environmental variables on compositional data. Axes indicate the variance proportion explained by respective PCoAs. Adonis test results, based on Bray–Curtis dissimilarity, are presented below each plot's title. Multivariate homogeneity of group dispersions (betadispersion), a prerequisite of permutational MANOVA, is also displayed. Mann–Whitney *U* test assessed significant differences in PCoA axes, richness, and diversity between dusty and clear conditions. Significance levels are indicated by symbols: '***' for <0.001, '**' for <0.01, '*' for <0.05, '.' for <0.1, and 'ns' for <1. (**B**, **E**) Richness plots exhibit species (**B**) and functional (**E**) richness, depicting the observed number of features, while (**C**, **F**) diversity plots display species (**C**) and functional (**F**) diversity using the Shannon–Wiener diversity index for the atmospheric microbiome under dusty and clear conditions. Pearson's correlation analysis explores the relationship between PM_{10} concentration (exclusive to dusty atmospheric conditions), temperature across all samples, and microbiome richness/diversity indices. Boxplots display median values (center lines), first and third quartiles (lower and upper hinges, 25th and 75th percentiles), while whiskers extend from hinges to values within 1.5 times the Interquartile Range (IQR). Outliers are red dots.

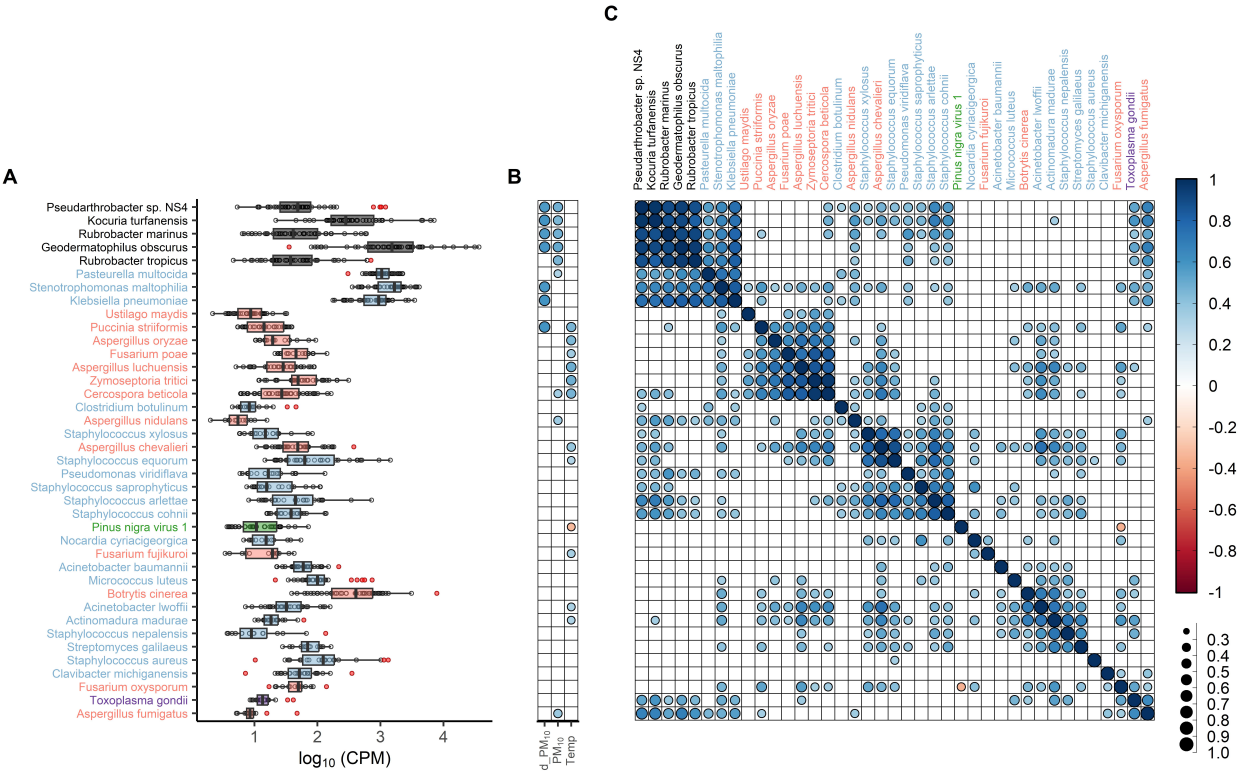

Fig. 2. Relationships among potential pathogens, dust-indicator taxa, and environmental variables. (**A**) Abundance distribution ($\log_{10}$(CPM)) for dust-indicator taxa and prevalent potential pathogens. Boxplot details: center lines represent medians, hinges display the 25th and 75th percentiles, while whiskers extend to values within 1.5 times the Interquartile Range (IQR) from the hinges. Red-colored dots indicate outliers. (**B**) Pearson's correlation analysis between individual taxa and environmental variables. 'd_PM_{10}' signifies the correlation between daily mean PM_{10} concentration specifically within dusty atmospheric conditions, while 'PM_{10}' denotes the correlation across all samples. 'Temp' represents the correlation between each taxon and the daily mean temperature. (**C**) Correlation matrix of Pearson's coefficients showing co-occurrence patterns between potential pathogens and dust-indicator taxa. Correlations with an absolute Pearson's coefficient (*r*) value above 0.3 and a P-value below 0.05, adjusted by the Benjamini–Hochberg method, were considered statistically significant. The visual representation uses color-coded correlation coefficient values and different-sized bins for ease of interpretation. Taxa names and boxplots are color-coded: black for dust-indicator taxa, light blue for bacteria, light red for fungi, green for viruses, and magenta for other eukaryotes. The x-axis and y-axis ordering were determined through hierarchical clustering using Ward's method with the ward.D option in the 'hclust' package. This method minimizes within-cluster variance and combines clusters based on the smallest between-cluster distance.

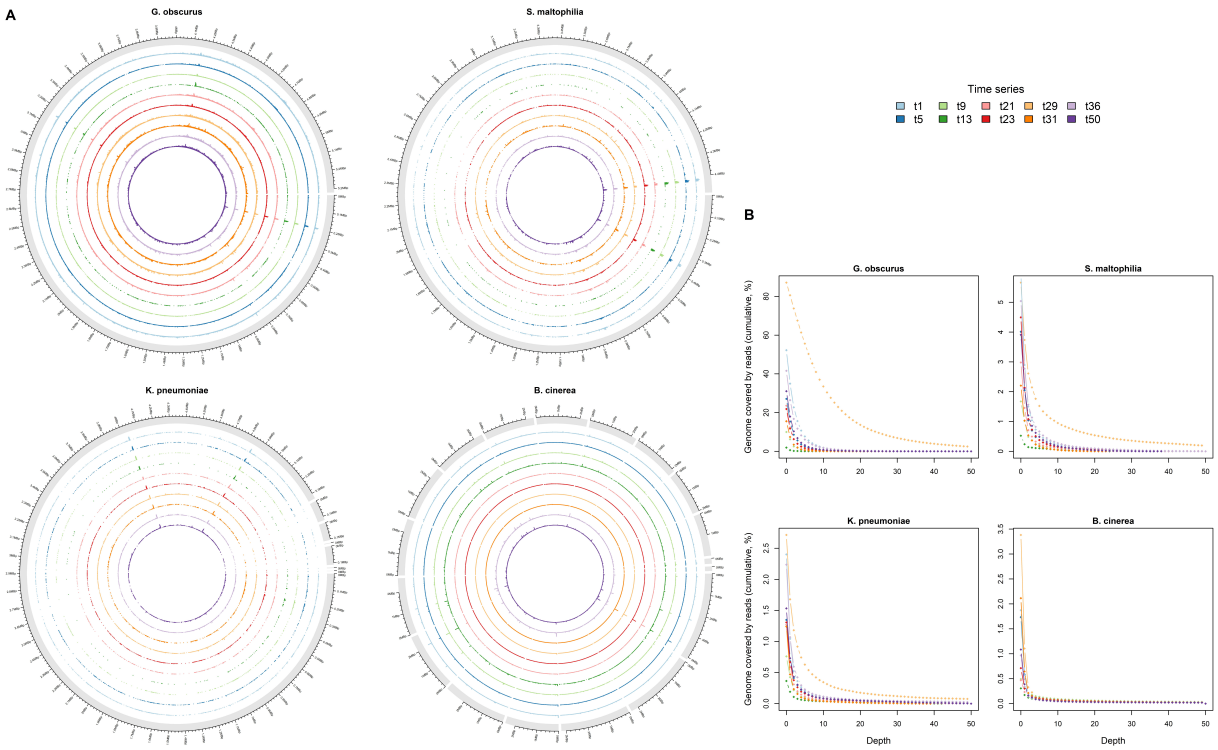

Fig. 3. Read mapping results of individual samples to reference genomes, demonstrating coverage and depth. (**A**) Circos display showcases the read mapping results for the most prevalent taxa across all samples, with *G. obscurus* serving as the reference, accompanied by the predominant bacterial pathogens *S. maltophilia* and *K. pneumoniae*, as well as the fungal pathogen *B. cinerea*. The outer circle represents the entire genome of each species, including chromosomes and plasmids, with a gap denoting the boundary. The genome size is annotated by numbers outside each circle. Inside, colored circles (bar plots) depict air samples collected under various atmospheric conditions. For visual convenience, only five clear days (t5, t13, t23, t31 and t50) and five dusty days (t1, t9, t21, t29 and t36) are shown here. Each aligned read within a sample to the reference genome is depicted as a colored bar, indicating its specific position in the reference genome, with the height of the bar representing the depth. (**B**) Coverage histograms illustrate the cumulative percentage of the total number of bases in the reference genome covered by different read depths. Detailed descriptions of atmospheric conditions from which air samples were obtained and comprehensive tables of the read mapping results of other prevalent pathogens are available in the Supplementary Materials.

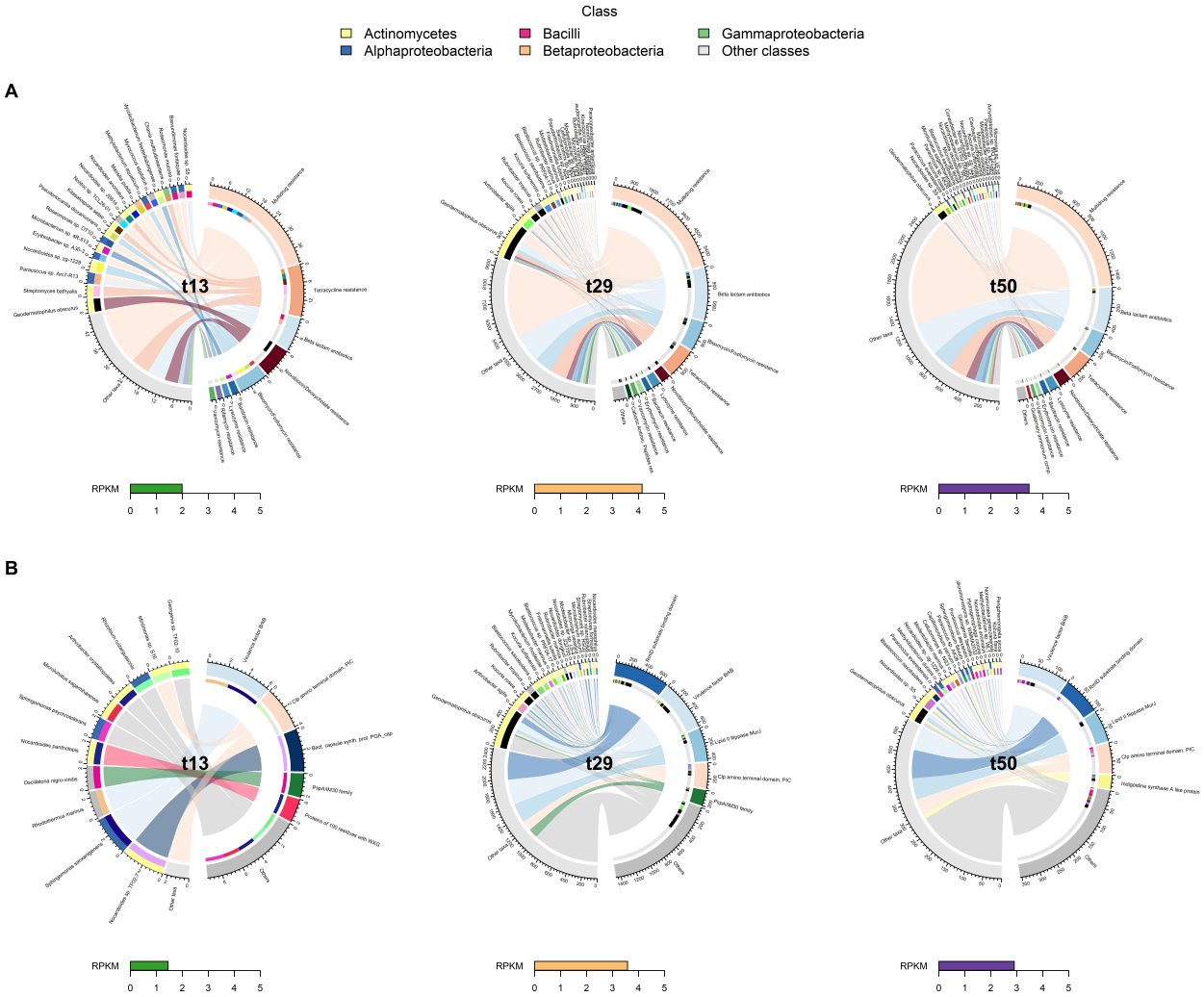

Fig. 4. Host microorganism carrying antimicrobial resistance and virulence-related genes in air samples under varying atmospheric conditions. The RPKM values of contigs associated with both taxonomy and antimicrobial resistance (**A**) and virulence-related traits (**B**) are annotated by numbers outside the circle. The sample name is displayed at the center of each chord diagram. For visual clarity, only three air samples representing clear (t13), dusty (t29), and high-temperature clear (t50) days are included. Inside the diagrams, colored sectors depict the top 20 species, top 10 antimicrobial resistance, and top 5 virulence-related traits with the highest RPKM values. The sum of the other taxa and functional features is depicted with a gray color code. The top 20 taxa are colored according to class and species level. Class level color codes (top section) are shown in the legend, while species level coloring (bottom section) represents dust-indicator taxa with a black color and the rest are colored randomly for each sample. The total $\log_{10}$(RPKM) values are presented as bar plots at the bottom of each chord diagram.